T H E U N I V E R S I T Y O F M I C H I G A N

COLLEGE OF ENGINEERING
Department of Engineering Mechanics
Department of Mechanical Engineering

Tire and Suspension Systems Research Group

Technical Report No. 8

BENDING CHARACTERISTICS OF CORD-RUBBER LAMINATES

S. K. Clark
D. H. Robbins

Project Directors: S. K. Clark and R. A. Dodge

ORA Project 02957

administered through:

OFFICE OF RESEARCH ADMINISTRATION ANN ARBOR

August 1961

ensm
UMR673

The Tire and Suspension Systems Research Group at
The University of Michigan
is sponsored by:

FIRESTONE TIRE AND RUBBER COMPANY

GENERAL TIRE AND RUBBER COMPANY

B.F. GOODRICH TIRE COMPANY

GOODYEAR TIRE AND RUBBER COMPANY

UNITED STATE RUBBER COMPANY

TABLE OF CONTENTS

LIST OF FIGURES

NOMENCLATURE

English Letters

a	Special case of ν.
A,B,C,D	Constants of integration in the general solution of the differential equation of deflection of a beam on an elastic foundation.
a_{ij}	Constants associated with generalized Hooke's law using properties based on complete cord tension or compression.
$\overline{D}_\xi, \overline{D}_\eta, \overline{D}$	Effective plate stiffnesses in bending.
$\overline{E}_\xi, \overline{E}_\eta, \overline{E}$	Elastic constants resulting from inversion of Hooke's law when shear strain is zero.
E_ξ, E_η, F	Elastic constants for orthotropic laminates with cords completely in tension or compression when shear strain is zero.
h	Ply thickness of each lamination in an orthotropic laminate.
k	Negative inverse of the radius of curvature.
k_f	Stiffness constant for an elastic foundation.
m	Bending moments per unit length applied to a specimen.
M	Total bending moment exerted on a specimen.
n	Half the total number of plies in a laminate.
N	Axial load per unit of circumference.
p	Total distributed load acting on the inside of a tubular specimen.
p_i	Internal pressure in the tubular cylinders.
P	Radial load per unit of circumference.
Q	Shear force exerted in the direction of the thickness of the wall of a tubular specimen.

s	Roots of the characteristic equation given by a beam on an elastic foundation.
t	Plate thickness of an orthotropic laminate.
w	Displacement in the ζ direction.
x,y,z	Orthogonal coordinates aligned along and normal to the cord direction.

Greek Letters

α	One-half the included angle between cords in adjoining plies in a two-ply laminate.
β,ν	Real and imaginary parts of the roots of the characteristic equation.
ϵ	Strain.
θ	Circumferential angle included between two different radii of the cylindrical specimens.
λ	A constant, $\lambda = \sqrt[4]{k_f/4\bar{D}_\xi}$.
ξ,η,ζ	Orthogonal coordinates aligned along and normal to the orthotropic axes of an orthotropic laminate.
σ	Stress.

FOREWORD

The properties of orthotropic laminates subjected to local bending stresses about symmetric axes have not yet been discussed in this series of reports. It is necessary to consider bending so that a quantitative measure of bending stiffness for this type of structure may be obtained. This result should be useful in formulating a strain-energy function for a toroidal shell and also for understanding the basic reaction of a cord-rubber laminate to bending stresses. This report is an attempt to apply the theory proposed in Ref. 1 to the bending problem.

SUMMARY

The classical theory of pure bending is used in conjunction with the generalized Hooke's law to develop an expression for the stiffness of laminated, orthotropic cord-rubber sheets which are subjected to bending deformations about symmetric axes of the structure. This stiffness may be predicted for a laminated structure with any number of plies and any angle between the cords of alternate plies if the four basic elastic moduli of a single ply are known.

Tests were run to determine the validity of the expressions predicting stiffness. The agreement between experiment and theory was good. The stiffness was found to be dependent on all four elastic constants, with the effects of extensional moduli and cross modulus particularly large.

ANALYSIS OF BENDING STIFFNESS

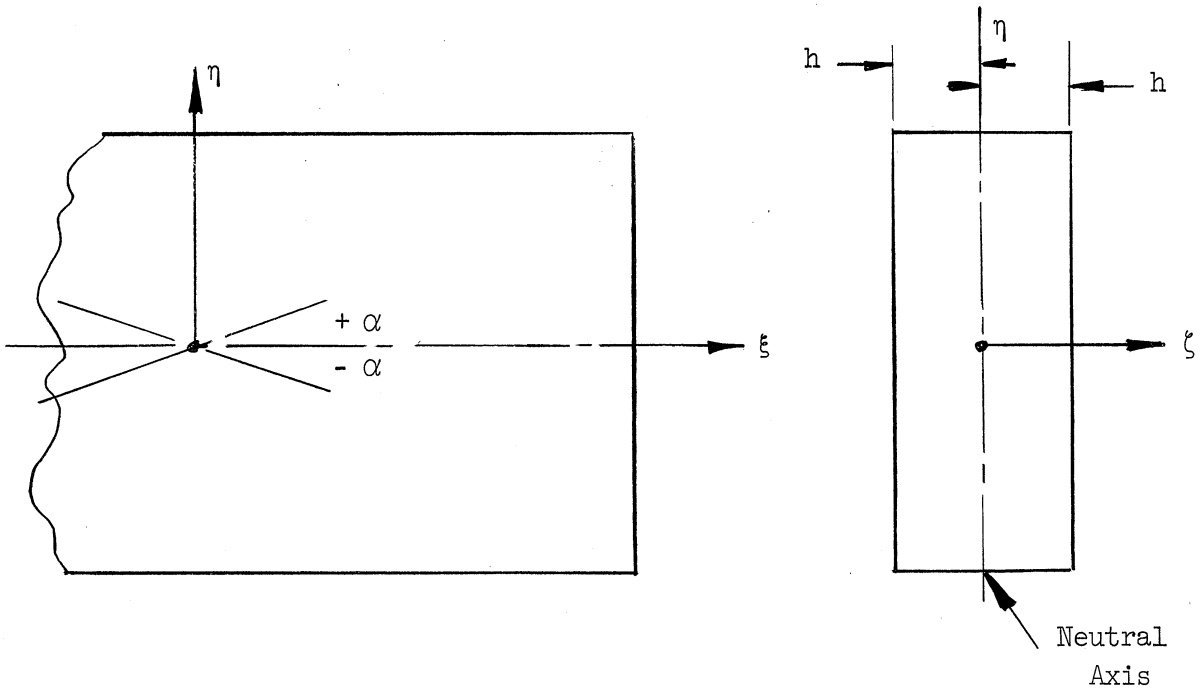

Fig. 1. Schematic view of a small section of a two-ply laminate.

Consider a two-ply laminate, as shown in Fig. 1, in which the cords are either completely in tension or completely in compression. The angles α are between ξ, a symmetric axis of the laminate, and the cord direction in an individual ply, $+\alpha$ for the cords of one ply and $-\alpha$ for the cords of the other. h is the thickness of a ply and ζ is an orthogonal coordinate in the direction of the laminate's thickness.

Assuming the cords all to have the same stiffness, say due to being preloaded into tension, let bending be about either of the symmetric axes ξ or η so that twist vanishes. From Ref. 1, the elastic law relating stress

and strain for each ply of Fig. 1 is:

$$\begin{aligned} \epsilon_\xi &= a_{11}\sigma_\xi + a_{12}\sigma_\eta + a_{13}\sigma_{\xi\eta} \\ \epsilon_\eta &= a_{21}\sigma_\xi + a_{22}\sigma_\eta + a_{23}\sigma_{\xi\eta} \\ \epsilon_{\xi\eta} &= a_{31}\sigma_\xi + a_{32}\sigma_\eta + a_{33}\sigma_{\xi\eta}. \end{aligned} \tag{1}$$

This is recognized as the generalized Hooke's Law. Due to the assumed symmetry of the deformation when bent about the ξ or η axis, the shear strain $\epsilon_{\xi\eta}$ due to twist must vanish. Hence, when σ_ξ and σ_η are applied, Eq. (1) becomes:

$$\begin{aligned} \epsilon_\xi &= a_{11}\sigma_\xi + a_{12}\sigma_\eta + a_{13}\sigma'_{\xi\eta} \\ \epsilon_\eta &= a_{21}\sigma_\xi + a_{22}\sigma_\eta + a_{23}\sigma'_{\xi\eta} \\ 0 &= a_{31}\sigma_\xi + a_{32}\sigma_\eta + a_{33}\sigma'_{\xi\eta} \end{aligned} \tag{2}$$

where $\sigma'_{\xi\eta}$ is the shearing stress necessary for strain compatibility between the plies. $\sigma'_{\xi\eta}$ acts on each ply and does not contribute directly to the bending moment about the neutral axis. The last of Eqs. (2) may be solved for $\sigma'_{\xi\eta}$, and this value may be inserted into the first two of Eqs. (2), giving

$$\begin{aligned} \epsilon_\xi &= \left(a_{11} - \frac{a_{13}^2}{a_{33}}\right)\sigma_\xi + \left(a_{12} - \frac{a_{13}a_{23}}{a_{33}}\right)\sigma_\eta \\ \epsilon_\eta &= \left(a_{21} - \frac{a_{21}a_{31}}{a_{33}}\right)\sigma_\xi + \left(a_{22} - \frac{a_{23}^2}{a_{33}}\right)\sigma_\eta. \end{aligned} \tag{3}$$

These may be inverted to yield

$$\sigma_\xi = \overline{E}_\xi \epsilon_\xi + \overline{F}\epsilon_\eta$$
$$\sigma_\eta = \overline{E}_\eta \epsilon_\eta + \overline{F}\epsilon_\xi \tag{4}$$

where

$$\overline{E}_\xi = \frac{\left(a_{22} - \frac{a_{23}^2}{a_{33}}\right)}{\left(a_{11} - \frac{a_{13}^2}{a_{33}}\right)\left(a_{22} - \frac{a_{23}^2}{a_{33}}\right) - \left(a_{12} - \frac{a_{13}a_{32}}{a_{33}}\right)^2}$$

$$\overline{E}_\eta = \frac{\left(a_{11} - \frac{a_{13}^2}{a_{33}}\right)}{\left(a_{22} - \frac{a_{23}^2}{a_{33}}\right)} \overline{E}_\xi \tag{5}$$

$$\overline{F} = -\frac{\left(a_{12} - \frac{a_{13}a_{23}}{a_{33}}\right)}{\left(a_{22} - \frac{a_{23}^2}{a_{33}}\right)} \overline{E}_\xi .$$

It might be noted here that the moduli $\overline{E}_\xi$, $\overline{E}_\eta$, $\overline{F}$ are dependent on the Young's moduli E_ξ and E_η and also on the cross modulus $F_{\xi\eta}$. By substitution of Eqs. (15) from Ref. 1 into Eq. (3) of this report, these relationships are found to be:

$$\overline{E}_\xi = \frac{E_\xi F_{\xi\eta}^2}{F_{\xi\eta}^2 - E_\xi E_\eta}; \quad \overline{E}_\eta = \frac{E_\eta F_{\xi\eta}^2}{F_{\xi\eta}^2 - E_\xi E_\eta}; \quad \overline{F} = -\frac{E_\eta E_\xi F_{\xi\eta}}{F_{\xi\eta}^2 - E_\xi E_\eta}. \tag{5a}$$

It is thus possible to predict $\overline{E}_\xi$, $\overline{E}_\eta$, and $\overline{F}$ knowing the elastic properties E_x, E_y, F_{xy}, and G_{xy} of a single sheet of orthotropic material.

In formulating a stiffness constant, the assumptions of pure bending of thin plates will be used; that is, it will be assumed that planes remain plane

and perpendicular to the axes η and ξ and that displacements and displacement gradients are small. On the basis of these assumptions, the strain-displacement relations for a plate are

$$\epsilon_\xi = -\zeta \frac{\partial^2 w}{\partial \xi^2} = -\zeta k_\xi$$

$$\epsilon_\eta = -\zeta \frac{\partial^2 w}{\partial \eta^2} = -\zeta k_\eta . \tag{6}$$

Equations (4) may now be rewritten

$$\sigma_\xi = -\zeta(\bar{E}_\xi k_\xi + \bar{F} k_\eta)$$

$$\sigma_\eta = -\zeta(\bar{E}_\eta k_\eta + \bar{F} k_\xi). \tag{7}$$

With reference to Fig. 1, the moments per unit length m_ξ and m_η may be formed by multiplying the appropriate stresses by the lever arm, $\zeta d\zeta$, and integrating from $(+nh)$ to $(-nh)$ where $2n$ is the total number of plies and h is the thickness of each ply. This is a generalization to $2n$ plies with alternating angles of $+\alpha$ or $-\alpha$. Previously only a two-ply structure was considered. It is justified by the fact that the stress distribution in any ply is given by Eq. (2), within the confines of the assumptions in force here. Thus,

$$m_\xi = \int_{-nh}^{+nh} \sigma_\xi \zeta d\zeta = -(\bar{E}_\xi k_\xi + \bar{F} k_\eta)\frac{2(nh)^3}{3}$$

$$m_\eta = \int_{-nh}^{+nh} \sigma_\eta \zeta d\zeta = -(\bar{E}_\eta k_\eta + \bar{F} k_\xi)\frac{2(nh)^3}{3}. \tag{8}$$

These may be written

$$\begin{aligned} m_\xi &= -\bar{D}_\xi k_\xi - \bar{D} k_\eta \\ m_\eta &= -\bar{D}_\eta k_\eta - \bar{D} k_\xi \end{aligned} \tag{9}$$

where

$$\bar{D}_\xi = \bar{E}_\xi \cdot \frac{2}{3}(nh)^3 = \bar{E}_\xi I, \tag{10a}$$

$$\bar{D}_\eta = \bar{E}_\eta \cdot \frac{2}{3}(nh)^3 = \bar{E}_\eta I, \tag{10b}$$

$$\bar{D} = \bar{F} \cdot \frac{2}{3}(nh)^3 = \bar{F} I \tag{10c}$$

represent the effective plate stiffnesses in beanding.

With knowledge of thickness and elastic properties of a single sheet of orthotropic material, a bending-stiffness constant can thus be predicted for a laminate of these sheets. The fact might again be recalled that this relationship is valid only if the cords in a cord-rubber laminate are either in tension or compression. The case in which some cords are in compression and some in tension will be taken up in a later report.

EXPERIMENTAL MEASUREMENT OF BENDING STIFFNESS

Some effort was expended in planning a test which would be particularly applicable to the clear demonstration of local bending rigidity in a cord-rubber laminate. Since only specimens of cylindrical shape were available, it seemed most direct to treat these as beams and to measure their deflection when loaded by end moments, such as shown in Fig. 2. However, this

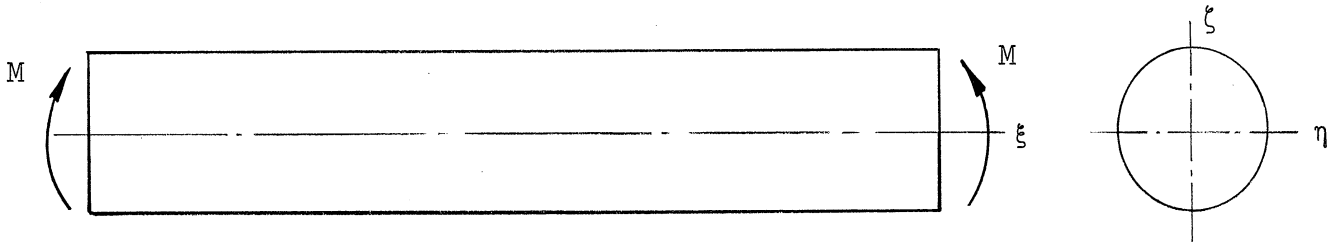

Fig. 2. Schematic view of a finite cylindrical tube loaded by end moments.

type of loading presented real difficulties in three areas:

(a) It was not possible to preload the cords without inducing frictional end moments which would have been difficult to measure accurately.

(b) The bending induced in the tube is in the form of a distribution of shell-membrane stresses around the tube, and is not composed of bending which is local in nature, so that the neutral axis lies inside the tube wall, between the two plies. It is desired to illustrate bending of this latter type, not the distribution of membrane forces.

(c) Early buckling of the tube wall would most certainly occur, since it is very thin.

For these reasons it was decided to attempt to demonstrate bending phenomena by use of a somewhat more novel and complicated scheme in which a radial line load is applied around the circumference of the tube by means of a constricting wire, such as is shown schematically in Fig. 3. This system also has the advantage of allowing the imposition of internal pressure and axial end loads in order to preload the cords. This problem is two-dimensional in the coordinates ξ and ζ as the deformation is symmetrical about the axis of the tube.

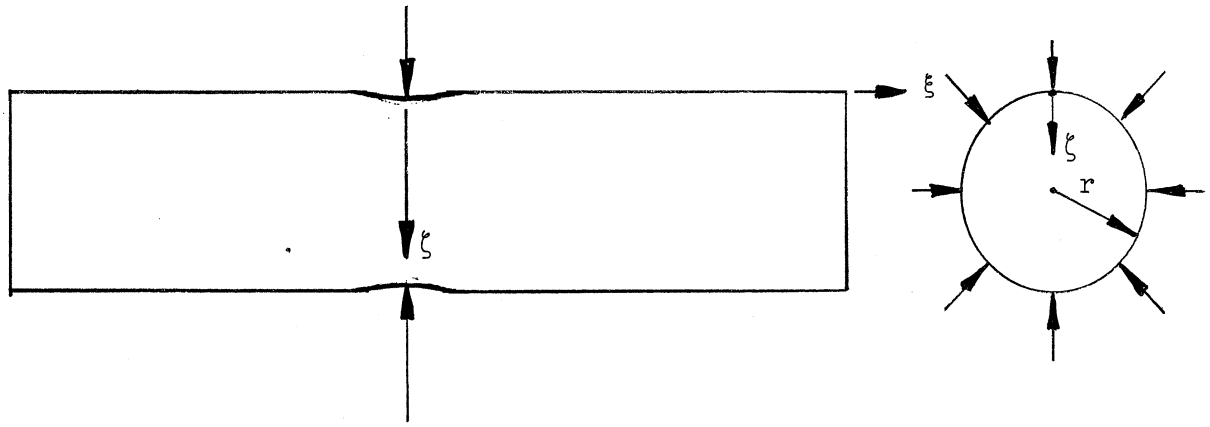

Fig. 3. Schematic view of a cylindrical tube under the action of radial line load applied on a circumference.

The bending rigidity of the tube walls may be derived from the solution for the radial deflection of the walls under this load. This problem is a relatively simple one in strength of materials, but its solution is quite lengthy and, for that reason, only the results will be presented here. The solution itself is thoroughly discussed in the Appendix. From the Appendix it may be shown that the bending stiffness is described, in a special case, by Eqs. (11).

If

$$N = 2\sqrt{\bar{D}_\xi \cdot k_f}\ , \tag{11a}$$

then

$$\bar{D}_\xi = k_f\left(\frac{P}{4p_i}\right)^4 \tag{11b}$$

in which N is the axial end load, P is the radial line load in pounds per inch, and p_i is the internal pressure. k_f represents a foundation stiffness proportional to the modulus of the tube in the circumferential direction, E_η, while $\bar{D}_\xi$ represents the bending rigidity in the longitudinal or axial direction. Equations (11) are valid only for a condition in which the axial load is set according to Eq. (11a), under which conditions the bending stiffness is given by Eq. (11b).

From Eqs. (11) it is clear that the determination of bending stiffness $\bar{D}_\xi$ is an iterative or cyclic process. It may also be seen that bending stiffness is dependent both upon the stiffness k_f and upon the fourth power of the radial load per unit pressure increase. This means that considerable care must be taken in experimental measurement since small fluctuations or errors in either measurement of the line load P or in measurement of the internal pressure could result in large variations of predicted bending stiffness.

The specimens used for these experiments were previously described in Ref. 1. These are four-ply 6-in.-diameter tubular specimens, with alternate cord angles being equal but opposite as is the usual construction practice, and they are shown in Fig. 4.

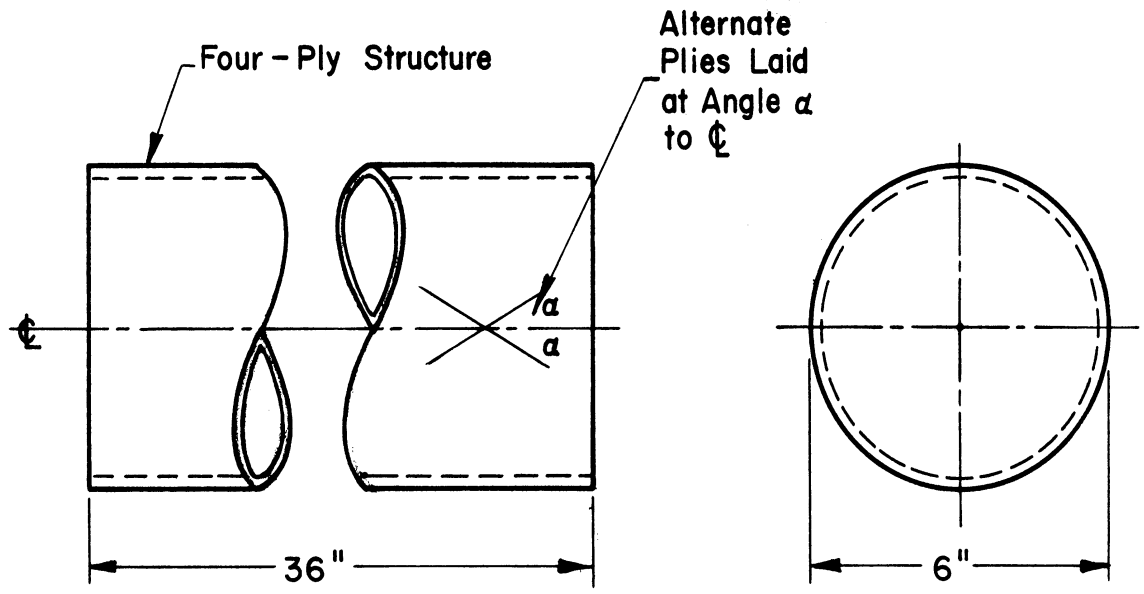

Fig. 4. Tubular test specimen showing dimensions.

The experimental procedure which was found necessary here began with the calculation of a value $\overline{D}_\xi$ for the particular specimen by use of Eqs. (10). This value was substituted into Eq. (11a), along with a measured value of the stiffness k_f. The resulting axial load N was found. Next, calculations were made to determine the values of axial load and internal pressure which, used together, resulted in proper loading of the cords in the specimen by means of the point Mohr's circle criterion described in Ref. 2.

The use of this Mohr's circle criterion also insured that angle changes would be quite small under the applied loads, thus removing the necessity for correcting data for angular change. Fortunately, the necessary value of end load N as predicted by Eqs. (11), when used in conjunction with the proper internal pressure as predicted from Mohr's circle as previously discussed, resulted in strains which were of the proper order of magnitude for the development of the full tension modulus of the textile cords. Table I shows

the strains used in the various experimental specimens described in this report.

TABLE I

α	0°	15°	30°	45°	60°
Cord Strain, per cent	0.3	0.3	0.3	0.4	1.3

The specimens were placed in a standard tensile testing machine using grips previously shown in Ref. 1, and the proper internal pressure and axial load were applied. This accomplished loading of the cords into a state of tension strain, as shown by Table I, as well as applying the necessary end load, as shown by Eq. (11a). At this point, a thin restraining wire was placed around the specimen with a small preload and its total length measured. Now internal pressure was caused to vary about this preset point. During this process a line load was generated in the wire due to expansion of the cylinder, and this load was measured by means of a load cell attached to the wire itself. A plot of the line load versus internal pressure, similar to that shown in Fig. 5 for a particular specimen, was then obtained for each specimen.

The slope of this curve was then determined and used in Eq. (11b) for calculation of a new stiffness $\overline{D}_\xi$. Generally, this calculated stiffness was quite close to or identical with the stiffness originally predicted from calculation, and only one or two successive iterations of the experimental process were necessary to cause convergence. This type of experiment was

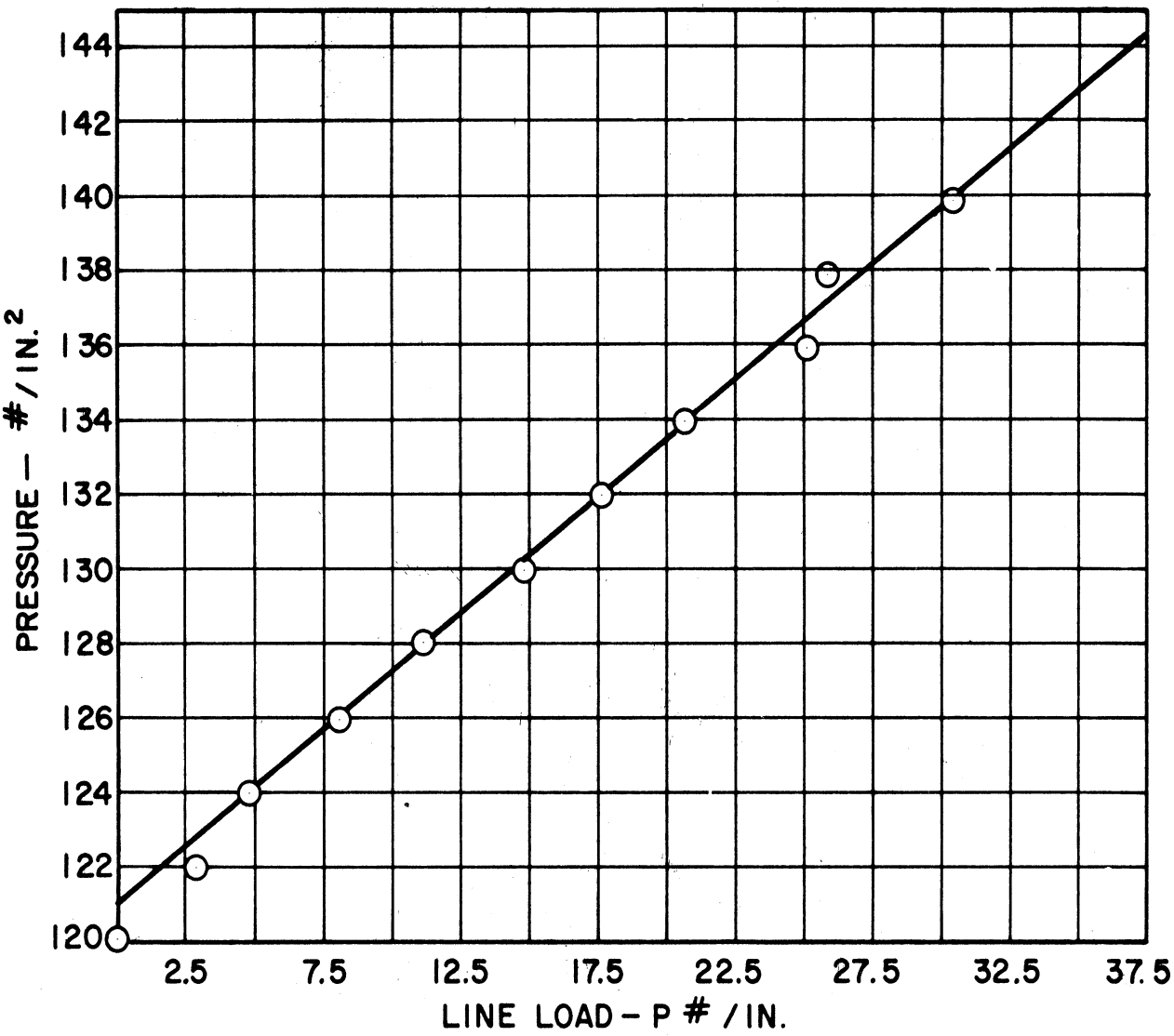

Fig. 5. Typical line load vs. pressure curve for cylindrical tubes subjected to constant axial loads and variable internal pressure with a restraining cable on a circumference.

performed on two samples at each of the cord angles shown in Table I, so that a total of twelve experimental points was obtained. The results of these are shown in Fig. 6 compared with the predicted values of stiffness obtained from Eqs. (10). Note that $\bar{D}_\xi(\alpha) = \bar{D}_\eta(\pi/2-\alpha)$.

Agreement between experiment and theory is relatively good, although a few substantial deviations from theory exist. In particular, the 45° spec-

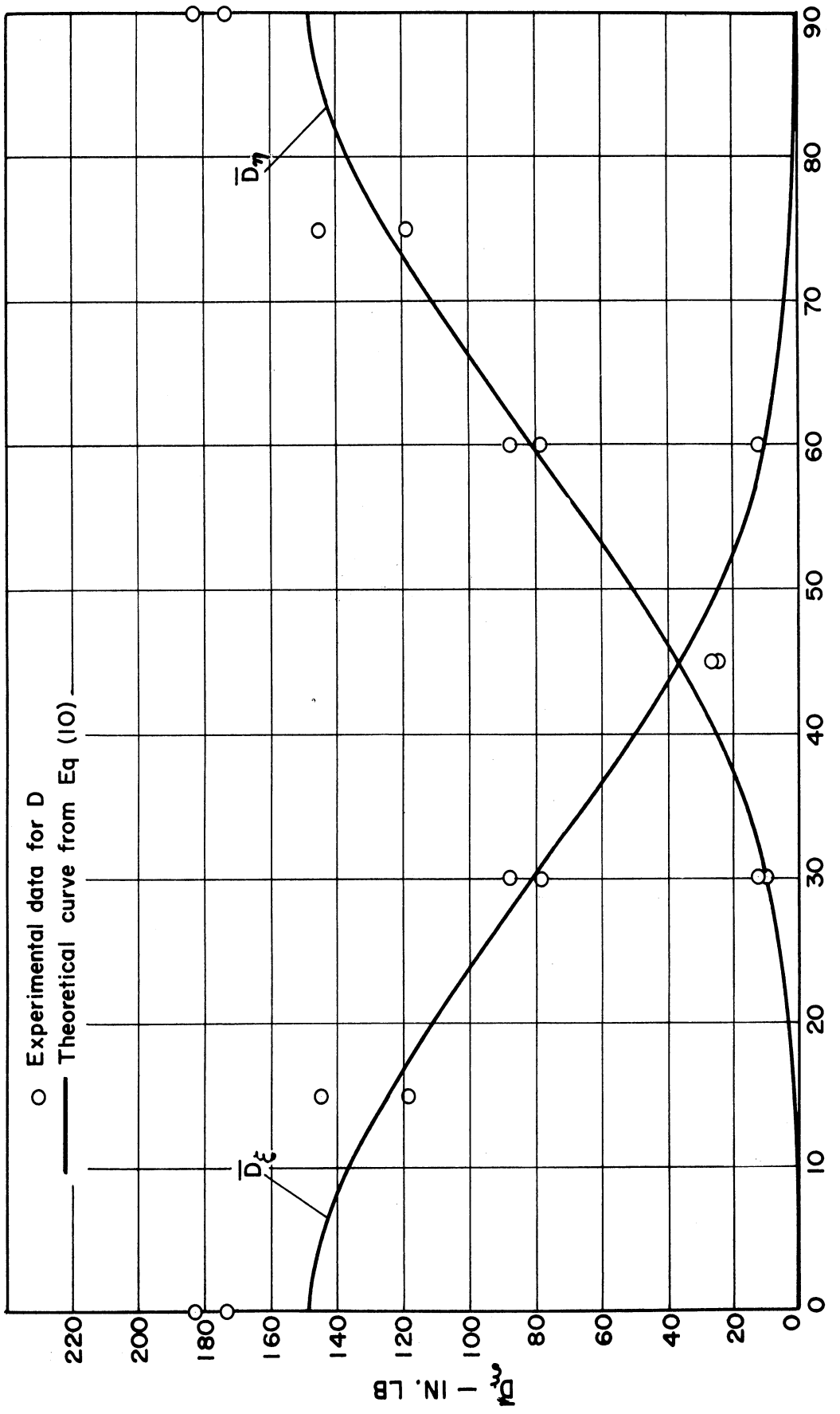

Fig. 6. Bending stiffnessess $\bar{D}_\xi$ and $\bar{D}_\eta$ as predicted from Eqs. (10a) and (10b) vs. cord angle α, along with experimental values of $\bar{D}_\xi$ and $\bar{D}_\eta$.

imens indicated bending stiffnesses somewhat lower than predicted by Eq. (10). In general, the fundamental difficulty in determining bending stiffness by the constriction of a cylindrical tube lies in the error propagation inherent in Eq. (11), where errors in measured quantities such as line loads or internal pressures are quadrupled due to the fourth-power dependence of bending stiffness on these line loads and pressures.

In view of this admittedly bad sensitivity, it is considered significant that agreement between experiment and theory was so close, and it is felt that this provides sufficient evidence to show that bending stiffness may indeed be predicted from Eqs. (10) with some accuracy.

EXPERIMENTAL INSTRUMENTATION

Since this is an unusual way of measuring bending stiffness, a description of the measuring techniques might be of interest. As mentioned earlier, the specimens were loaded in a standard Riehle screw-type tensile testing machine. Internal pressure was provided by bottled nitrogen, using both a 7-foot mercury manometer and a 150-pound Bourdon-tube pressure gauge in the line. For lower-pressure work the manometer was switched on, while for high-pressure work it was cut out of the system. Axial loads ranged from 1800 to 2500 pounds, while internal pressure ranged from 10 in. Hg to 140 psi, depending on the specimens being tested. Specimens with low cord angle generally required larger end loads and lower pressures, while the 60° specimens used very large internal pressures coupled with compressive end forces. The specimen in the testing machine is shown in Fig. 7.

The constricting cable was 1/16-in. flexible aircraft control cable wound once around the specimen and connected through a turn-buckle on one end into a 500-lb Baldwin load cell. The other end of the cable was attached to the opposite end of the load cell. This load cell rode on a track so that translation of the specimen could occur without inducing load in the constricting wire. Using this mechanical arrangement, changes in diameter of the specimen were the only causes of load in the wire.

Figure 8 is a sketch of this measuring system and the constricting wire, and Fig. 9 is a photograph of the arrangement. A scale attached to the cable

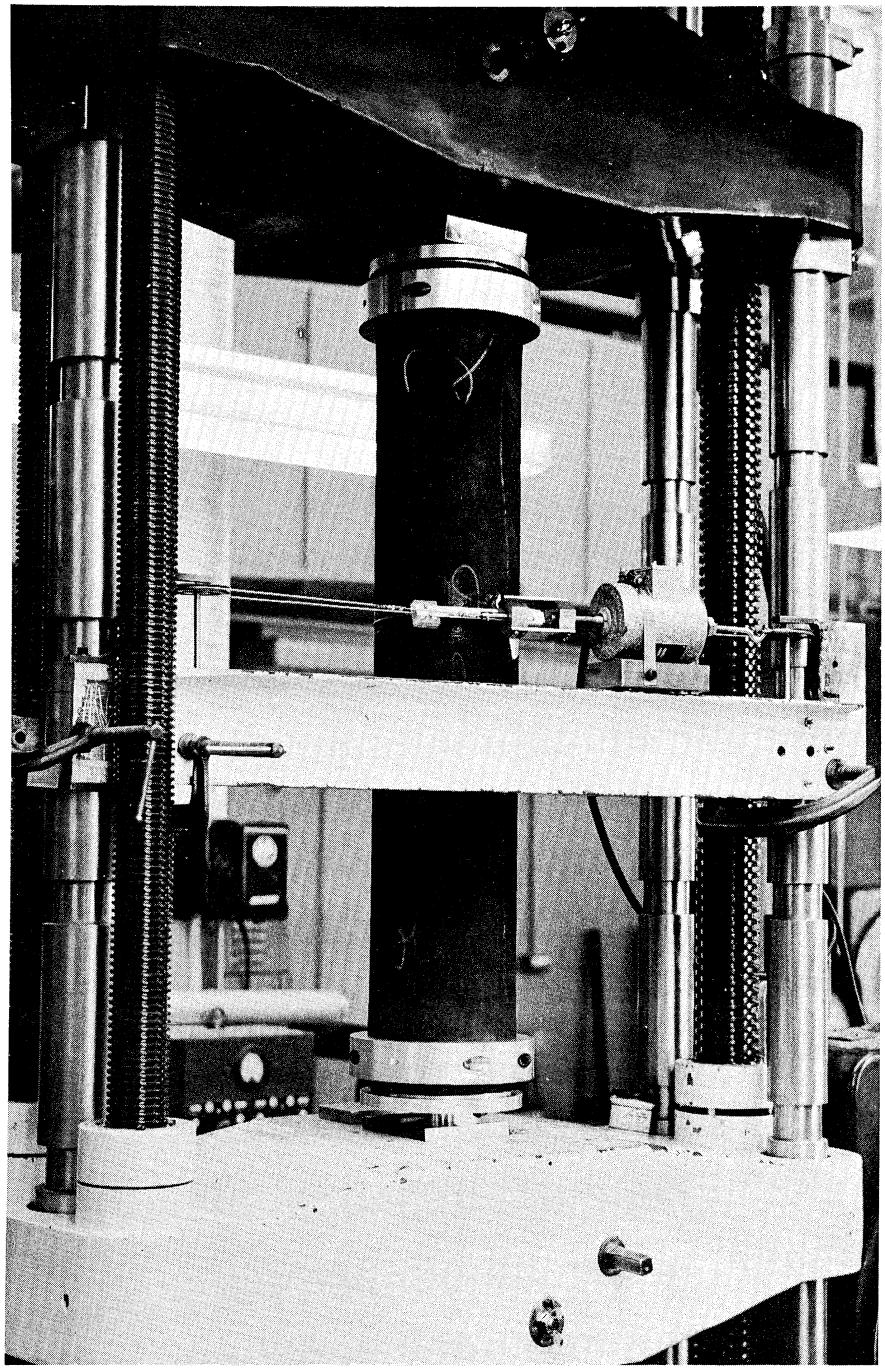

Fig. 7. Photograph of specimen in testing machine.

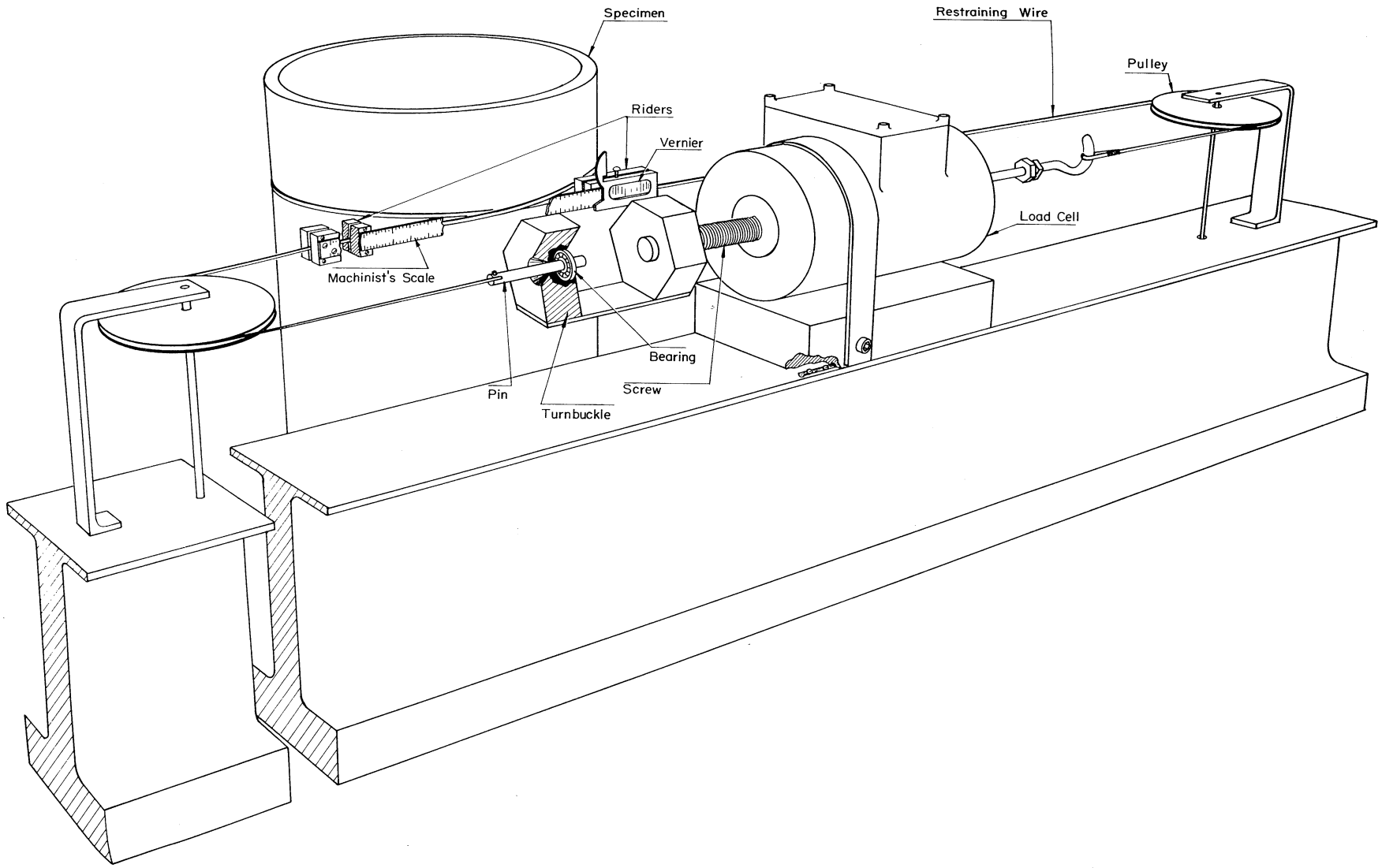

Fig. 8. Schematic view of the measuring system and the constricting cable.

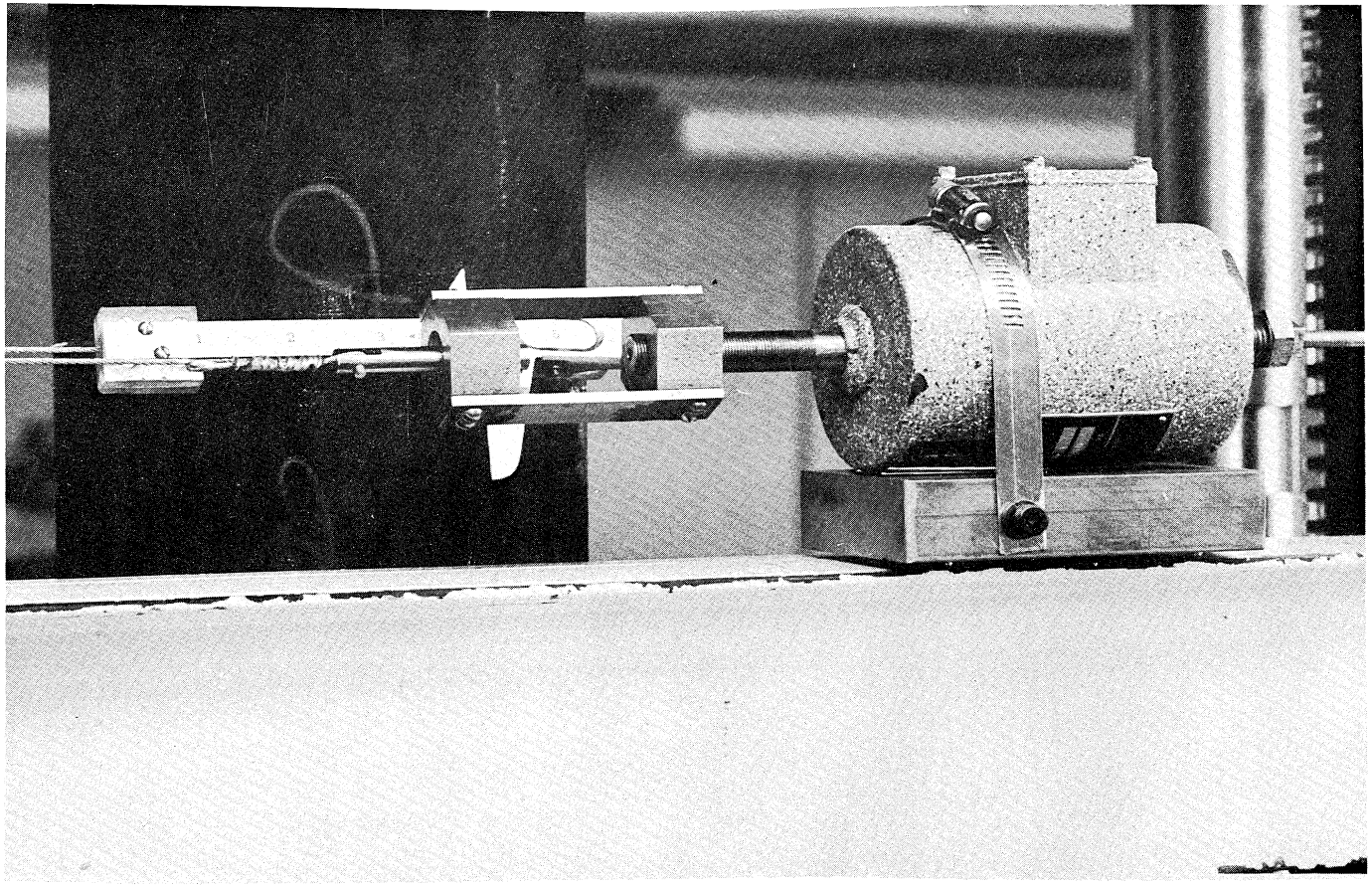

Fig. 9. Photograph of the measuring system and the constricting cable.

was used to measure the change in circumference of the specimen. When the radius of the specimen was to be kept constant at the point of application of the line load, the turn-buckle was used to adjust the system for stretch of the cable.

APPENDIX

Consider an element of a plate with unit width as shown in Fig. 10. This might be a strip from a cylindrical shell if the ratio of plate thickness to radius is quite small. The moment equilibrium equation may be written

$$M + dM - M + N d\zeta - Q d\xi = 0.$$

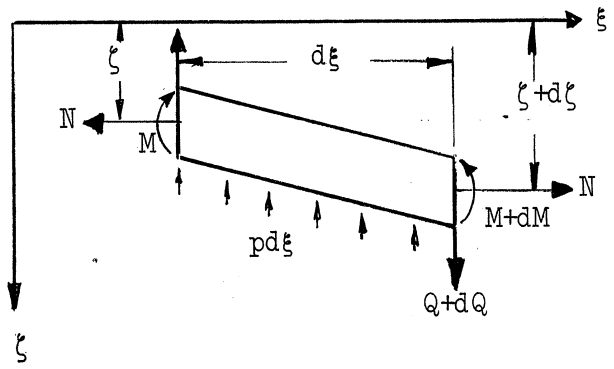

Fig. 10. Free-body diagram of a differential strip from a cylindrical shell under the action of forces and moments.

This may be differentiated twice.

$$\frac{d^2M}{d\xi^2} + N \frac{d^2\zeta}{d\xi^2} - \frac{dQ}{d\xi} = 0.$$

It will be recalled from elementary bending theory that

$$M = -\bar{E}_\xi I \frac{d^2\zeta}{d\xi^2} = -\bar{D}_\xi \frac{d^2\zeta}{d\xi^2}.$$

Note that

$$p d\xi = k_f \zeta d\xi + p_i d\xi$$

where k_f is the spring constant of the elastic foundation model and p_i is the internal pressure on the cylinder. The assumption is made that the cylinder responds to a load as if it were a mass of springs. The equilibrium equation may be written

$$\bar{D}_\xi \frac{d^4\zeta}{d\xi^4} - N \frac{d^2\zeta}{d\xi^2} + k_f\zeta = -p_i. \qquad (a)$$

For the homogeneous problem let $\zeta = Ae^{s\xi}$. s is the solution of the equation,

$$s^4 - \frac{N}{\bar{D}_\xi} s^2 + \frac{k_f}{\bar{D}_\xi} = 0 \qquad (b)$$

$$s = \pm\sqrt{\frac{N}{2\bar{D}_\xi} \pm i\sqrt{\frac{k_f}{\bar{D}_\xi} - \left(\frac{N}{2\bar{D}_\xi}\right)^2}}$$

Case I: $N < 2\sqrt{k_f\bar{D}_\xi}$

The quantity under the inner square root is positive. s might thus be written as a complex number,

$$s_{1,2,3,4} = \pm \nu \pm i\beta,$$

where

$$\nu = \sqrt{\sqrt{\frac{k_f}{4\bar{D}_\xi}} + \frac{N}{4\bar{D}_\xi}}; \quad \beta = \sqrt{\sqrt{\frac{k_f}{4\bar{D}_\xi}} - \frac{N}{4\bar{D}_\xi}}; \quad \lambda = \sqrt[4]{\frac{k_f}{4\bar{D}_\xi}}. \qquad (c)$$

The general solution is

$$\zeta = Ae^{\nu\xi} e^{i\beta\xi} + Be^{-\nu\xi} e^{i\beta\xi} + Ce^{\nu\xi} e^{-i\beta\xi} + De^{-\nu\xi} e^{-i\beta\xi}$$

or

$$\zeta = \left[C_1 e^{\nu\xi} + C_2 e^{-\nu\xi}\right] \cos \beta\xi + \left[C_3 e^{\nu\xi} + C_4 e^{-\nu\xi}\right] \sin \beta\xi.$$

For the particular integral, the solution $\zeta = A$ is assumed and substituted into (a), from which

$$A = -p_i/k_f.$$

The complete general solution is written

$$\zeta = -\frac{p_i}{k_f} + \left[C_1 e^{\nu\xi} + C_2 e^{-\nu\xi}\right] \cos \beta\xi + \left[C_3 e^{\nu\xi} + C_4 e^{-\nu\xi}\right] \sin \beta\xi.$$

The boundary conditions are now applied. At $\zeta(\infty)$ the only deflection is due to internal pressure.

$$\zeta(\infty) = -\frac{p_i}{k_f}. \tag{d1}$$

Also, the bending moment must vanish there:

$$\left(\frac{d^2\zeta}{d\xi^2}\right)_{\xi=\infty} = 0. \tag{d2}$$

These conditions imply $C_1 = C_3 = 0$. If only the positive half beam ($\xi > 0$) is considered, the other two boundary conditions are

$$Q(0) = -\frac{P}{2} = \bar{D}_\xi \left(\frac{d^3\zeta}{d\xi^3}\right)_{\xi=0}, \tag{d3}$$

(where P is the line load applied at the origin). Also, the slope will be zero at the origin, so that

$$\left(\frac{d\zeta}{d\xi}\right)_{\xi=0} = 0. \tag{d4}$$

Substitution into the solution gives

$$C_4 = \frac{P}{4} \frac{1}{\bar{D}_\xi \beta(\beta^2 + \nu^2)}, \qquad C_2 = \frac{P}{4} \frac{1}{\nu(\beta^2 + \nu^2)\bar{D}_\xi},$$

and the elastic deflection line for Case I is

$$\zeta = -\frac{p_i}{k_f} + \frac{P}{2\nu\beta} \frac{\lambda^2}{k_f} e^{-\nu\xi} \left[\beta \cos \beta\xi + \nu \sin \beta\xi\right] \tag{e}$$

Case II: $N > 2\sqrt{k_f \bar{D}_\xi}$

β of the previous discussion may be replaced by $i\bar{\beta}$, where

$$\bar{\beta} = \sqrt{\frac{N}{4\bar{D}_\xi} - \sqrt{\frac{k_f}{4\bar{D}_\xi}}}\,. \tag{f}$$

In this case, the constants C_2 and C_4 become

$$C_4 = \frac{P}{4} \frac{1}{\bar{D}_\xi i\bar{\beta}(\nu^2 - \bar{\beta}^2)}, \qquad C_2 = \frac{P}{4} \frac{1}{\nu(\nu^2 - \bar{\beta}^2)\bar{D}_\xi},$$

and

$$2\lambda^2 = \nu^2 - \bar{\beta}^2 .$$

The elastic line for Case II is thus written

$$\zeta = -\frac{p_i}{k_f} + \frac{Pe^{-\nu\xi}}{8\nu\bar{D}_\xi \lambda^2} \left[\cosh \bar{\beta}\xi + \frac{\nu}{\bar{\beta}} \sinh \bar{\beta}\xi\right]. \tag{g}$$

Case III: $N = 2\sqrt{k_f \bar{D}_\xi}$

In this case, ν reduces to a and β vanishes.

$$a = \sqrt{\frac{N}{2\bar{D}_\xi}}\,; \qquad \beta = 0. \tag{h}$$

Substitution into the general solution yields the deflection line

$$\zeta = -\frac{p_i}{k_f} + \frac{P}{4\bar{D}_\xi a^3} e^{-a\xi}(1 + a\xi). \qquad \text{(i)}$$

Little has previously been written about the relationship of the beam on the elastic foundation to cylindrical shells. Timoshenko (Ref. 3) shows that the two problems are identical since the shell walls act as an elastic foundation. For the tubular shell, the hoop strain ϵ_h is proportional to the radial displacement ζ if the radial strain is uniform across any cross section. Thus,

$$\epsilon_h = \frac{\zeta}{r}.$$

where r is the tube radius. A radial displacement thus generates a hoop strain related to the hoop stress by

$$\sigma_h = E_\eta \frac{\zeta}{r} = \frac{\sigma_{hu}}{t} = E_\eta \frac{\zeta}{r};$$

$$\sigma_{hu} = \frac{E_\eta t}{r}$$

where σ_{hu} is the hoop load per unit width. There must be a relationship between σ_{hu} and the radial line load which caused it. Consider the equilibrium of the shell segment shown in Fig. 11.

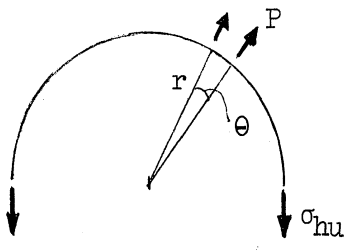

$$\int_0^\pi Pr \sin\theta d\theta = 2\sigma_{hu}$$

$$= Pr[-\cos\theta]_0^\pi = 2Pr$$

$$P = \frac{\sigma_{hu}}{r}$$

Fig. 11. Free-body diagram showing the equilibrium between the constricting cable and the membrane hoop stresses in the cylindrical shell.

Thus the line load may be written

$$P = \frac{\sigma_{hu}}{r} = \left[\frac{E_n t}{r^2}\right] \zeta \, . \qquad (j)$$

This relation expresses deflection in terms of the load. The proportionality factor is the radial stiffness, k_f, of the structure.

$\bar{D}_\xi$ is obtained by solving a deflection line equation for $\bar{D}_\xi$ when $\zeta(0)$ is used as an experimentally determinable variable. For Cases I and II,

$$\bar{D}_\xi = \frac{1}{4k_f^3}\left\{\frac{P^2}{4\left[\zeta(0) + \frac{p_i}{k_f}\right]^2} - Nk_f\right\}^2 \, . \qquad (k)$$

This expression might be useful in some cases, but in general the experiments could not be performed accurately enough to warrant its use. Subtraction of numbers nearly the same size magnifies errors, as does the process of raising to powers. Case III seemed to offer fewer problems and was finally accepted as the basis for experiments. Here it is necessary to satisfy the two equations

$$N = 2\sqrt{k_f \bar{D}_\xi} \; ; \qquad \zeta(0) = -\frac{p_i}{k_f} + \frac{P}{4\bar{D}_\xi a^3} \, .$$

If the radius is held constant at zero deflection,

$$\zeta(0) = 0, \qquad (l)$$

and thus

$$\frac{p_i}{k_f} = \frac{P}{4\bar{D}_\xi a^3} \, .$$

Solving for $\bar{D}_\xi$ yields

$$\bar{D}_\xi = \frac{2N^3 p_i^2}{r^2 P}$$

but, as this is Case III

$$N = 2\sqrt{k_f \overline{D}_\xi} \; ; \tag{m}$$

so, eliminating N,

$$\overline{D}_\xi = k_f \left(\frac{P}{4p_i} \right)^4 . \tag{n}$$

Thus, in running any experiments in Case III bending the relationships (l) and (m) were followed as closely as possible with the experimental variables being P and p_i.

ACKNOWLEDGMENT

The instrumentation for this experiment was designed and constructed by Mr. N. L. Field. Mr. D. A. Dodge and Mr. Richard N. Dodge assisted in obtaining experimental data.

REFERENCES

1. S. K. Clark, The Plane Elastic Characteristics of Cord-Rubber Laminates, Univ. of Mich. Res. Inst. Technical Report 02957-3-T, Ann Arbor, Michigan.

2. R. N. Dodge, N. L. Field, and S. K. Clark, The Plane Elastic Characteristics of Cord-Rubber Laminates - II, Univ. of Mich. Res. Inst. Technical Report 02957-7-T, Ann Arbor, Michigan.

3. S. Timoshenko, Strength of Materials, Vol. II, D. Van Nostrand Co., New York, 1959.

DISTRIBUTION LIST

	No. of Copies
The General Tire and Rubber Company Akron, Ohio	6
The Firestone Tire and Rubber Company Akron, Ohio	6
B.F. Goodrich Tire Company Akron, Ohio	6
Goodyear Tire and Rubber Company Akron, Ohio	6
United States Rubber Company Detroit, Michigan	6
S. S. Attwood	1
R. A. Dodge	1
The University of Michigan ORA File	1
S. K. Clark	1
Project File	10

UNIVERSITY OF MICHIGAN
3 9015 02827 4986